MODELING CO_2 INJECTION AT CRANFIELD, MISSISSIPPI: INVESTIGATION OF METHANE AND TEMPERATURE EFFECTS

Christine Doughty and Barry Freifeld

Lawrence Berkeley National Laboratory
#1 Cyclotron Rd.
Berkeley, California, USA, 94720
e-mail: cadoughty@lbl.gov; bmfreifeld@lbl.gov

ABSTRACT

A large-scale carbon dioxide (CO_2) injection pilot is ongoing at Cranfield, Mississippi, in a saline aquifer where the brine has high dissolved methane (CH_4) content. The pilot site includes one injection well and two observation wells, all with extensive monitoring. The breakthrough of CH_4 and CO_2 at the observation wells provides important insights into phase partitioning and the multipath nature of flow through the storage formation. Injected CO_2 is cooler than the ambient formation temperature, making temperature a potentially important observation as well.

Simulations of the first year of CO_2 injection were conducted using an axisymmetric (RZ) model, with layering based on well logs obtained from the injection well. The equation of state module EOS7C was used, which, unlike the more commonly used module ECO2N, allows temperatures as high as the ambient temperature at Cranfield, about 126–128°C. EOS7C treats CO_2, CH_4, and water, but does not include salt or a salinity dependence on CO_2 solubility. Although the simplification of an RZ model precludes study of those aspects of the pilot test relating to formation dip or lateral heterogeneity, its simple structure enables us to focus on physical processes involving the phase partitioning of CH_4 and CO_2, and temperature effects. Key observations that the model should reproduce include the arrival of a bank of free-phase CH_4 ahead of the main CO_2 plume at each observation well, and nonmonotonic changes in CH_4 and CO_2 mass fraction as a function of time at the observations wells, suggesting that multiple distinct flow paths exist between the injection well and the observation wells, each with its own bank of free-phase CH_4 leading the CO_2. Another interesting feature is the action of buoyancy flow to segregate the much less dense gaseous CH_4 from the supercritical CO_2. Thermal effects that would occur even if the injected CO_2 were at the same temperature as the formation include Joule-Thomson cooling, cooling accompanying water evaporation into the CO2-rich phase, and heating accompanying CO_2 dissolution into the aqueous phase. The bulk cooling arising from the relatively cool (~95°C) CO_2 itself can also provide insight into CO_2 behavior. As the cool CO_2 moves through the formation, it is heated by the existing brine and rock that it passes through; thus, the thermal front lags far behind the actual extent of the CO_2. Examining this lag quantitatively may provide information on the nature of the flow paths through the formation.

INTRODUCTION

A large-scale CO_2 injection pilot is currently under way at Cranfield, Mississippi, in a brine-saturated formation adjacent to an oil field where CO_2 injection is being used for enhanced oil recovery (EOR), operated by Denbury Onshore LLC (Figure 1). CO_2 injection into a 25 m thick saline aquifer known as the Tuscaloosa Formation, at ~3.2 km depth, started in December 2009. The initial injection rate was 3 kg/s, which was subsequently increased to 5 and then 9 kg/s. Two monitoring boreholes were installed approximately 72 m and 98 m from the injector. The gas composition, consisting mainly of CO_2, CH_4, and injected tracers (SF_6 and Kr), was measured frequently in the monitoring boreholes via U-tube (Freifeld et al., 2005) sampling with on-site mass spectroscopy. The pressure in the injection borehole was also monitored at a high temporal rate. In addition, the distribution of gas saturation with depth was measured via well logging before and twice during the injection, using a pulsed neutron reservoir saturation tool (RST). The geophysical datasets included elec-

trical resistance measurements (ERT) and a pair of traditional time-lapse crosswell seismic surveys (Hovorka et al., 2011). Other researchers have made detailed models of the site (e.g., Hoesseni et al., 2012; Doetsch et al., 2012) in order to match various observation datasets. Here a simplified axisymmetric model is used, to enable focus on the physical processes involving CO_2, CH_4, and heat transfer.

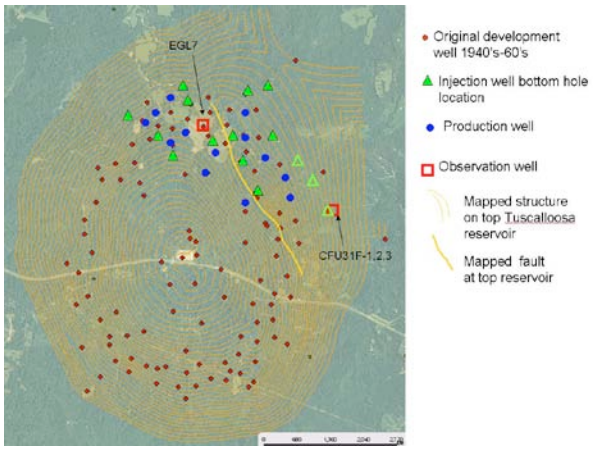

Figure 1. Plan view of Denbury's Cranfield EOR operation. Contours show the elevation of the top of the storage formation. The CO_2 injection pilot well field is identified by the red box labeled CFU31F-1,2,3.

NUMERICAL SIMULATOR AND EQUATION OF STATE

The results shown here are obtained from the numerical simulator TOUGH2 (Pruess et al., 1999; Pruess, 2004) and the equation-of-state module EOS7C (Oldenburg et al., 2004). TOUGH2 is a numerical simulation program for nonisothermal flows of multiphase, multicomponent fluids in permeable (porous or fractured) media. Fluid flow is modeled with Darcy's law extended for two-phase flow via relative permeability and capillary functions. TOUGH2 employs the integral-finite-difference method for spatial (Narasimhan and Witherspoon, 1976) discretization. For regular geometries, this method is equivalent to a simple finite-difference method, whereas for complicated geometries, it has all the flexibility of a finite-element method. TOUGH2 solves fully coupled fluid-flow and heat-flow equations, using implicit time-stepping. The resulting discrete nonlinear algebraic equations for mass and energy conservation are written in a residual form and solved using Newton/Raphson iteration.

EOS7C is a fluid-property module for the TOUGH2 simulator (Version 2.0) that was developed for applications involving geologic storage of CO_2 in formations containing water and methane. It includes a comprehensive description of the thermodynamics and thermophysical properties of H_2O-CO_2-CH_4 mixtures that reproduces fluid properties largely within experimental error for the temperature and pressure conditions of interest. In particular, CO_2 and CH_4 can exist in a gas-like phase (CO_2 is actually supercritical if pressure and temperature are above the critical point (72 bars, 31°C) or dissolved in the aqueous phase, and water can evaporate into the gas-like phase. Due to its numerical formulation, some CH_4 must be present in every gridblock, but the presence of dissolved CH_4 in saline aquifers associated with hydrocarbon production is reasonable. EOS7C also allows a tracer to partition between the aqueous and gas phase. In its present form, EOS7C does not consider salt, although such a capability is currently under development (C. Oldenburg, personal communication, 2012). Additionally, EOS7C does not account for the heat of dissolution of CO_2, but simulations (Han et al., 2012) using ECO2N have shown that this effect is much smaller than other thermal effects (Joule-Thomson cooling and the cooling that accompanies the evaporation of water) occurring when CO_2 is injected into a saline aquifer.

Many simulations of GCS use equation of state module ECO2N (H_2O-CO_2-NaCl; Spycher and Pruess, 2005; Pruess and Spycher, 2007) and are thus limited to temperatures below about 110°C, but EOS7C allows temperatures as high as the ambient temperature at Cranfield, about 126–128°C. Additionally, the inclusion of CH_4 in EOS7C is important, because initial conditions at Cranfield are CH_4-saturated brine and, as will be seen in the results section below, the breakthrough of CH_4 and CO_2 at the observation wells provides important insights into the multipath nature of flow through the storage formation.

MODEL DEVELOPMENT

Figure 2 shows the permeability profiles inferred from well-logs of the injection well. Vertical discretization of the model was chosen to

capture all the important variability in the permeability profile, which results in 20 model layers, each 1.2 m thick, for a 24 m thick storage formation. Because log information is given with 0.5 foot (0.15 m) resolution, averaging must be done to assign model properties. Horizontal permeability for the model is obtained by arithmetic averaging of the well-log permeabilities, and vertical permeability is obtained by harmonic averaging of the well-log permeabilities. The notable minimum in permeability at 3093-3094 m depth is inferred to be caused by a shale baffle.

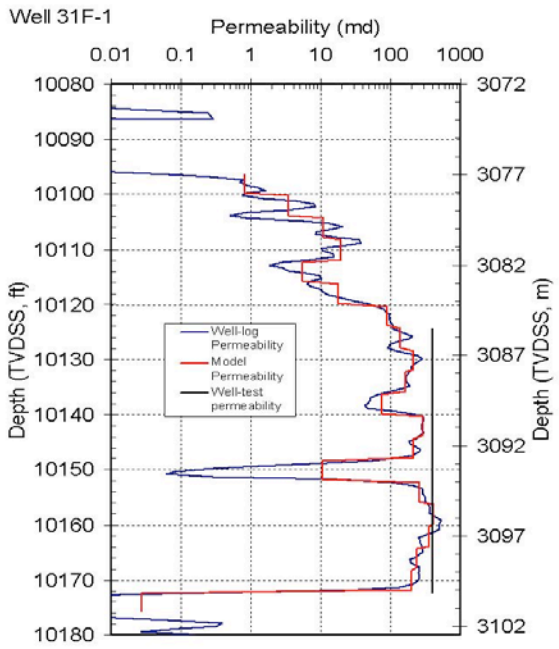

Figure 2. Permeability inferred from well log (blue symbols) and average values used for model (red lines). The black bar shows the perforated interval and the formation-average permeability inferred from a well test. Depths are true vertical depth subsea (TVDSS).

The fact that the well test yielded an average permeability for the storage formation consistent with the higher well-log permeabilities suggests that the high-permeability channels between shale baffles, if not individually continuous, are at least well-connected.

The well logs actually just provide information on porosity, so permeability is inferred by examining the permeability-porosity relationship obtained from sidewell core, as shown in Figure 3. Note that sidewell core samples do not provide information for samples with porosity greater than about 0.25, as these samples are not well recovered by the sidewall coring process. For the model, a curve fit is made to the sidewall core porosity-permeability relationship for porosities up to 0.25, and is then extrapolated to the larger porosity values (up to about 0.35) observed in the well logs.

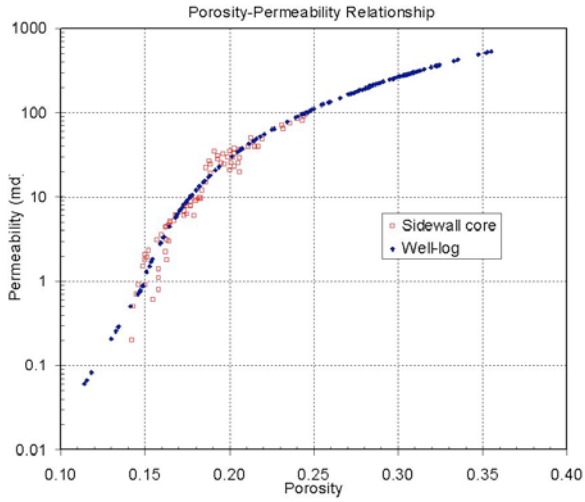

Figure 3. Permeability and porosity measured in sidewall core (red) and the curve fit used to assign permeability for the well-log porosities (blue).

No site-specific information is used for characteristic curves. Instead, functional forms and parameters for capillary pressure and relative permeability are taken from literature values for other Gulf Coast geologic settings (Holtz, 2005; Doughty et al., 2008). Liquid relative permeability uses the van Genuchten (1980) model with $m = 0.65$, and gas relative permeability is quasi-linear (Figure 4). Residual liquid saturation S_{lr} decreases as permeability increases, according to $S_{lr} = 0.2464 - 0.0945 \log(k)$, where k is permeability in millidarcies (M. Holtz, personal communication, 2003), with a minimum value of 0.05. Capillary pressure uses the van Genuchten model with $n = 1.4$, and strength P_{c0} inversely proportional to the square root of permeability, with $P_{c0} = 0.188$ bars for $k = 100$ md. Hysteresis is included in the characteristic curves (IRP = ICP =12, Doughty, 2007, 2009), but since only the injection period is modeled, and injection rate is modeled as monotonically increasing, imbibition is not significant.

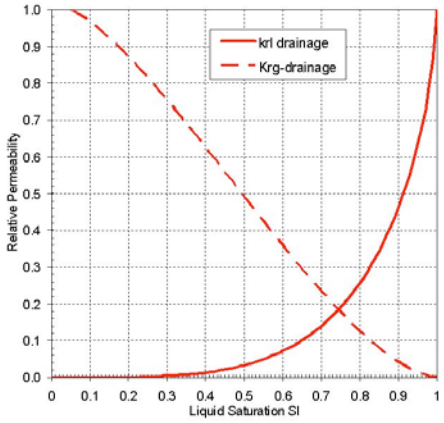

Figure 4. Relative permeability curves for the smallest value of S_{lr} used. For larger values of S_{lr}, the curves are shifted to the right, but the general shape remains the same.

Formation dip is small enough (1–2 degrees) to make an axisymmetric model reasonable for the injection period. This geometry would not be so good for modeling a post-injection rest period, since significant up-dip migration would be expected for the high-permeability sands, even for a slightly dipping storage formation.

Radial grid spacing starts fine at the well and gradually increases to 4 km, where a constant-property boundary is imposed (Figure 5).

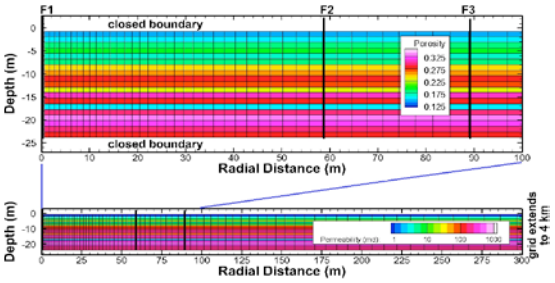

Figure 5. Axisymmetric grid used for the simulations.

The top and bottom boundaries of the model are closed. This is a good approximation for the fluid-flow boundary condition, since cap and bedrock permeabilities are very low. It is not so good for heat flow, however, because heat transfer between the confining layers and formation may be significant, especially for longer times. Future simulations will consider this process by adding the semi-analytical solution by Vinsome and Westerveld (1980) embodied in the Qloss subroutine in TOUGH2, invoked with MOP(15).

Initial conditions for CO_2 injection consist of a water-saturated formation at constant temperature (126°C) and hydrostatic pressure (about 300 bars). The water is saturated with dissolved CH_4 (X_{CH4L} = 0.00285). The hydrostatic pressure distribution is created by temporarily closing the outer radial boundary of the model and running the simulation with no sources or sinks until a steady pressure distribution develops.

The step-wise constant-injection-rate schedule used for the model (Figure 6) corresponds to the first six months of the actual injection at Cranfield, which is extrapolated for the rest of the year. Overall, the amount of CO_2 injected is about right compared to the actual amount. Throughout the injection period, injection consists of 98.5% mass fraction CO_2 and 1.5% mass fraction CH_4. This amount of CH_4 is sufficient to enable the code to run smoothly, is comparable to what was measured at Cranfield, and is typical of with natural CO_2 sources that may not be highly pure. The injection temperature is held fixed at 96°C (by specifying a large heat capacity), which is accurate for the early part of the injection period, but somewhat high for later times when the injection rate increased. Tracer slugs were added to the injected CO_2 at three times (Figure 6).

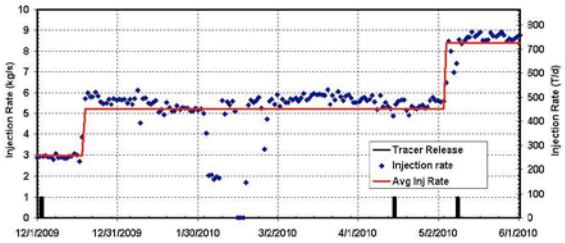

Figure 6. Cranfield injection rate and step-wise approximation used for model. The times of three tracer releases are also shown.

Injection is modeled with a mass source in each model layer, with the fraction of fluid going into each layer proportional to the permeability of that layer. It would be more correct to inject all the CO_2 in the top layer and assign high vertical permeability to all gridblocks representing the well to enable injection of CO_2 throughout the formation according to the pressure difference

between the well and the formation at each layer. This procedure usually works well for isothermal problems; however, it can cause numerical instabilities when the heat flow equation is also solved, so it was not done for the present simulations. Because the column of CO_2 in the well has lower density (~800 kg/m^3) than a column of water in the formation (~1000 kg/m^3), the static pressure profiles in the two columns differ, but the injection interval is only about 14 m thick here, so the pressure difference will be only about 0.3 bars—small compared to the pressure increase accompanying injection (~55 bars), so the error introduced is small.

SIMULATION RESULTS

Time-Series at Observation Wells

Figure 7 shows the modeled gas saturation, and CO_2, CH_4, and SF_6 mass fractions in the gas phase for the two observation wells F2 and F3, during the first 50 days of CO_2 injection, obtained by averaging over the model layers 3-19, which represent the open interval in the observation wells. The model predicts the arrival of a bank of gaseous CH_4 ahead of the super-critical CO_2. This phenomenon has been predicted before (Oldenburg and Doughty, 2011) and reflects the fact that although under ambient conditions, all the CH_4 can be dissolved in the water, as soon as a gas phase is present, much of the CH_4 evaporates into it. The SF_6 tracer also preferentially partitions into the gas phase, and arrives nearly coincidentally with the CH_4.

The corresponding U-tube data is also shown in Figure 7. The U-tubes in both wells became clogged shortly after injection began, and did not operate until the arrival of CO_2 (which proved to be an excellent solvent for cleaning the U-tubes) at about 11 and 15 days in Wells F2 and F3, respectively. Thus the first arrival of CH_4 and SF_6 was not monitored, but the fact that the first CH_4 and SF_6 measurements show a decreasing trend while the first CO_2 measurements show an increasing trend supports the model result for the arrival of a bank of free-phase CH_4 ahead of the CO_2. The model arrival time is just a few days late for Well F2, but is about 15 days late for the more distant Well F3, suggesting that the actual flow field is not well approximated by the radial symmetry of the model, but that CO_2 is travelling in more linear preferential paths.

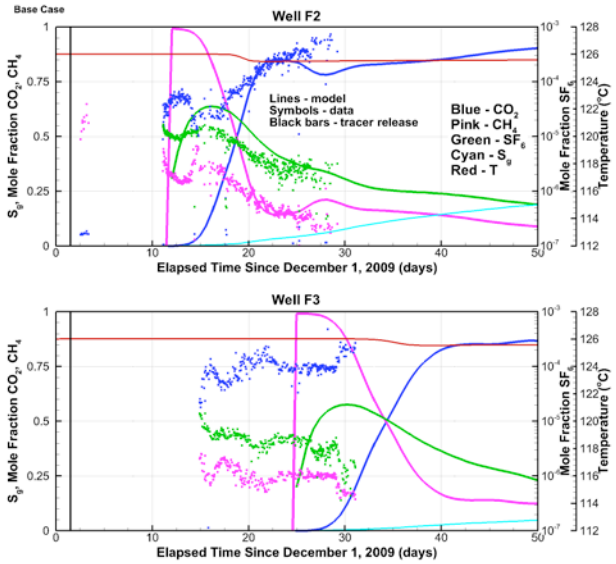

Figure 7. Modeled temperature (T), gas saturation (S_g), and CO_2, CH_4, and SF_6 mass fractions in the gas phase for the two observation wells F2 and F3 for the first 50 days of CO_2 injection. Note that SF_6 is plotted on a log scale.

Both the model and U-tube data show CH_4 and CO_2 mass fractions that oscillate in time. We interpret this as the arrival at different times of injected CO_2 travelling through distinct flow paths. For the RZ model, the only distinct flow paths are those above and below the shale baffle (see Figure 2), but for the field, there could be multiple flow paths in all three dimensions.

Figure 7 also shows modeled temperature at layer 17, which is the layer with the highest permeability, and the first layer to show a temperature response. There is a small temperature drop (~0.5°C) coincident with the arrival of the gas phase at each well, which is interpreted as Joule-Thompson cooling accompanying expansion of CO_2 as it moves away from the injection well (i.e., from higher to lower pressure) and cooling resulting from the evaporation of water into the CO_2-rich phase . Both of these effects would occur even if the injected CO_2 had the same temperature as the formation. The large temperature decrease corresponding to the low temperature of the injected CO_2 (30°C lower than the formation temperature), begins to be

felt at Well F2 at about 160 days (Figure 8), far behind the saturation-front arrival at 12 days. This delay occurs because the CO_2 thermally equilibrates with the brine and formation rock it comes in contact with as it moves away from the injection well. The heat capacity of these components is significant enough that the model predicts the thermal front has not even reached Well F3 within the first year.

Given the late arrival of CO_2 predicted for Well F3 (28 days versus the actual 15 days), the thermal prediction for Well F3 is not expected to be accurate. Based on geological understanding and the quick CO_2 arrival at Well F3, actual CO_2 flow paths are inferred to be localized laterally in contrast to the radial symmetry of the current model. In fact, comparing model and actual temperature arrivals may provide additional information about the nature of the CO_2 flow paths. Many small flow paths would be retarded by the thermal equilibration with their surroundings much more than a few large flow paths, and hence their thermal signature could be well-predicted by the axisymmetric model, even if the arrival of the CO_2 itself were not. In contrast, for a few large flow paths, neither the CO_2 arrival nor the thermal arrival would be well-predicted by an axisymmetric model. Unfortunately, the temperature gauges in Wells F2 and F3 did not function properly, so direct comparison with field measure temperatures has not been possible.

Figure 8 also enables comparison of the SF_6 peaks for all three tracer releases. The first peak, for tracer released just after CO_2 injection began, is much sharper than the latter two peaks, which is consistent with the widely accepted notion that a two-phase plume growing in a single-phase region develops a self-sharpening front. The model matches all peak heights and arrival times for Well F2 reasonably well, but for F3 the model arrivals are not only too late (as expected based on the late CO_2 arrival), but the latter peak is also too low and wide, not even resolving the individual peaks of the latter two tracer releases. This is consistent with the hypothesis that the flow occurs through limited preferential flow paths, rather than spreading radially as in the model.

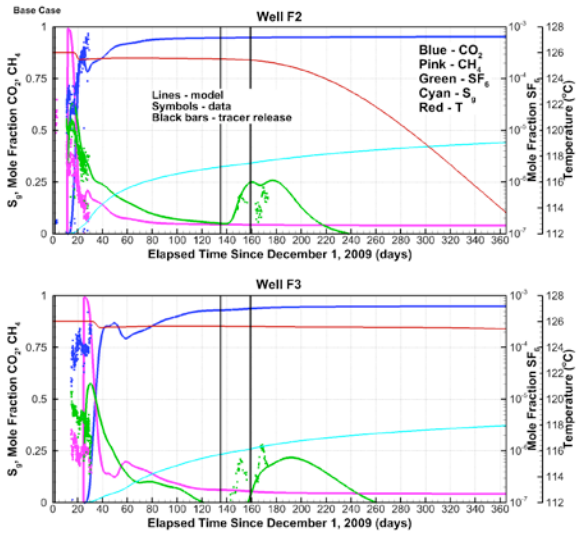

Figure 8. Modeled temperature (T), gas saturation (S_g), and CO_2 and CH_4 mass fractions in the gas phase for the two observation wells F2 and F3 for the entire year of CO_2 injection. Note that SF_6 is plotted on a log scale.

Spatial Distributions

Spatial distributions (r-z cross sections through the axisymmetric model) at 10, 60, and 365 days are shown in Figures 9, 10, and 11 and provide further insights into the physical processes occurring as supercritical CO_2 is injected into a CH_4-saturated brine. The uppermost frame in each figure shows the model porosity distribution. Because permeability increases as porosity increases, this distribution identifies the highest permeability regions in yellow and orange, and the saturation distribution (second frame) indicates that the CO_2 is moving preferentially into the upper portion of these regions. In particular, the low-permeability shale baffle at $z \sim -16$ m ($z = 0$ is the top of the model) divides the CO_2 plume into two parts. Pressure changes are relatively small for this high-permeability formation, but pressure changes extend far beyond the CO_2 plume itself. Note that the temperature scale is non-uniform: most of the range (96°C–125°C) is shown in colors from blue to yellow—this identifies the cooling attributed to the cool temperature of the injected CO_2. From 125°C to 126°C (orange to red), the scale is greatly expanded, to show the small temperature decreases attributed to Joule-Thompson cooling and the evaporation of water.

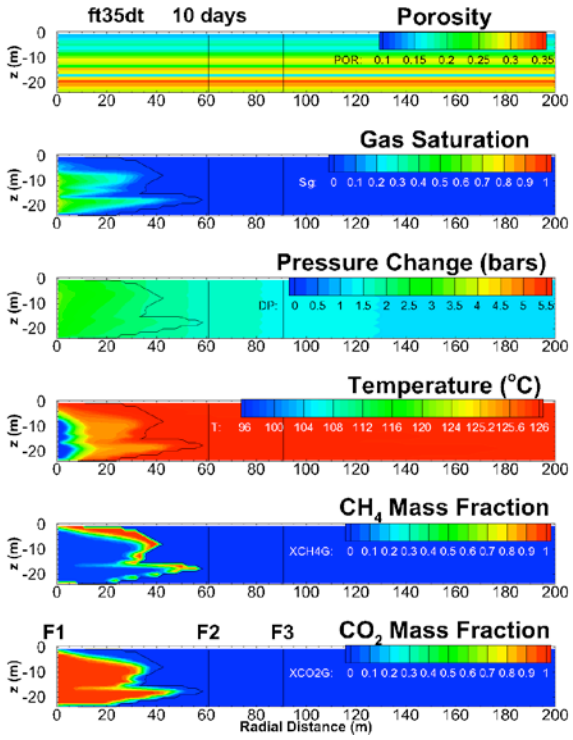

Figure 9. Model results after 10 days of CO_2 injection. In each frame the black contour line shows $S_g = 0$.

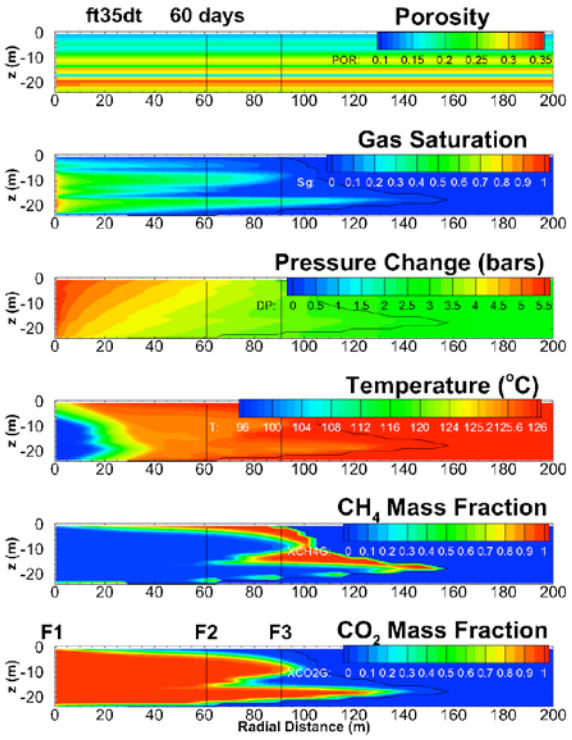

Figure 10. Model results after 60 days of CO_2 injection. In each frame the black contour line shows $S_g = 0$.

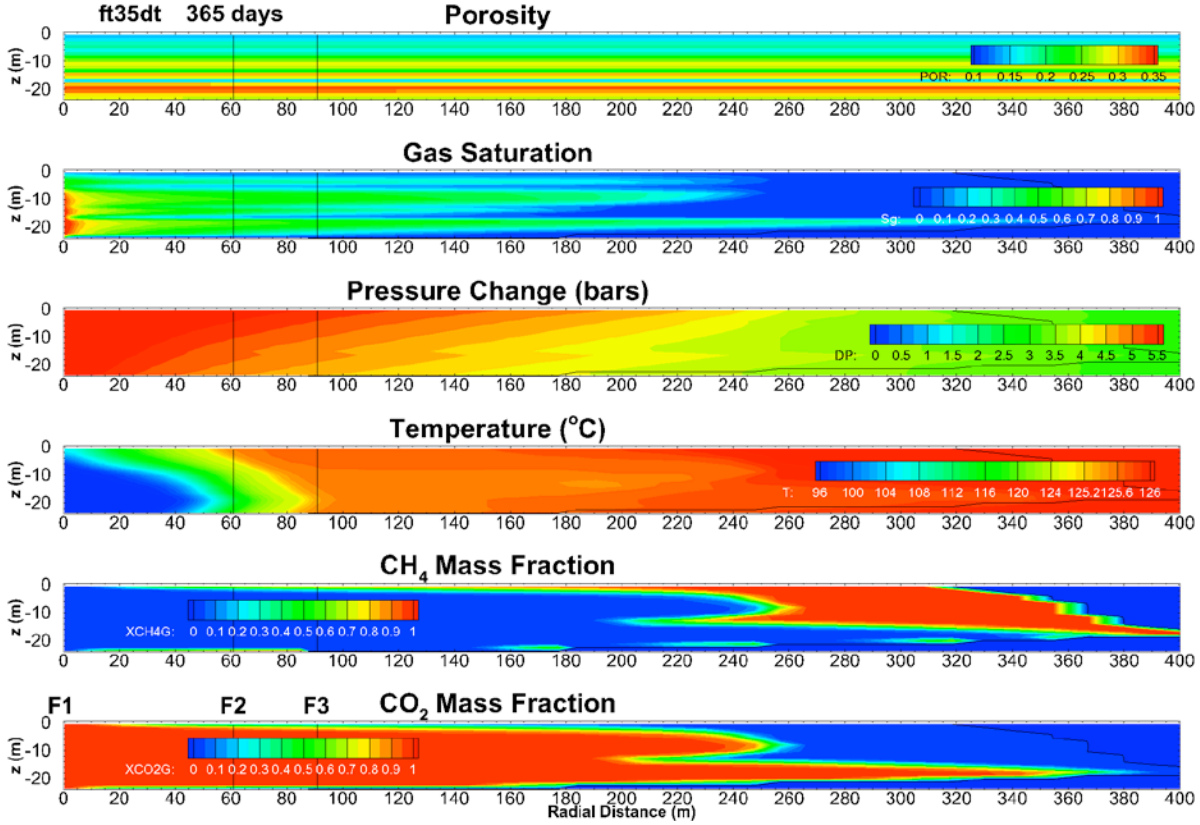

Figure 11. Model results after 365 days of CO_2 injection. In each frame, the black contour line shows $S_g = 0$.

The CH_4 and CO_2 mass fraction plots illustrate how the initially dissolved CH_4 evaporates when the CO_2 arrives and is pushed ahead of the main CO_2 plume. Since the CH_4 has very low density, it is strongly buoyant, and by 365 days it has all moved to the upper portion of the formation.

CONCLUSIONS AND FUTURE WORK

This simplified modeling of the Cranfield CO_2 injection pilot has proved to be an extremely valuable exercise for gaining insight into the physical processes accompanying CO_2 injection into CH_4-saturated brine. The interplay of multiphase flow effects and formation heterogeneity creates distinct signatures of multiple flow paths, something rarely directly observed in the field. Current extensions of this work include a 3D model with lateral heterogeneity, and incorporation of more realistic relative permeability functions, derived from laboratory experiments with Tuscaloosa Formation core samples.

ACKNOWLEDGMENT

We acknowledge Denbury for hosting the CO_2 injection pilot and Sue Hovorka of Texas Bureau of Economic Geology for guiding the project. Funding is through SECARB (Southeast Carbon Sequestration Partnership), provided by the National Energy Research Laboratory, US Department of Energy, Office of Fossil Energy. LBNL is funded under DOE Contract Number DE-AC02-05CH11231.

REFERENCES

Doetsch, J., M.B. Kowalsky, C. Doughty, S. Finsterle, J.B. Ajo- Franklin, X. Yang, C.R. Carrigan, and T.M. Daley, *Towards fully coupled hydrogeophysical inversion of CO2 migration data in a deep saline aquifer*, SEG-AGU Hydrogeophysics workshop, Boise, ID, July 2012.

Doughty, C., Modeling geologic storage of carbon dioxide: comparison of hysteretic and non-hysteretic curves, *Energy Conversion and Management*, 48(6), 1768-1781, 2007.

Doughty, C., *User's Guide for Hysteretic Capillary Pressure and Relative Permeability Functions in iTOUGH2*, Rep. LBNL-2483E, Lawrence Berkeley National Laboratory, Berkeley, CA, 2009.

Doughty, C., B.M. Freifeld, and R.C. Trautz, Site characterization for CO2 geologic storage and vice versa – the Frio brine pilot, Texas, USA as a case study, *Environmental Geology*, 54(8), 1635-1656, 2008.

Freifeld, B.M R.C. Trautz, Y.K. Kharaka, T.J. Phelps, L.R. Myer, S.D. Hovorka, and D.J. Collins, The U-tube: A novel system for acquiring borehole fluid samples from a deep geologic CO2 sequestration experiment, *Journal of Geophysical Research*, 110, B10203, 2005.

Han, W.S., K.-Y. Kim, E. Park, B.J. McPherson, S.-Y. Lee, M.-H. Park, Modeling of spatiotemporal thermal response to CO_2 injection in saline formations: Interpretation for monitoring, *Transport in Porous Media,* 93, 381–399, 2012.

Hosseini, S.A., H. Lashgarib , J.W. Choi, J.-P. Nicot, J. Lua, and S.D. Hovorka, *Static and Dynamic Reservoir Modeling for Geological CO2 Sequestration at Cranfield, Mississippi, U.S.A,* Texas Bureau of Economic Geology, Austin, TX, 2012.

Holtz, M.H., *Reservoir characterization applying residual gas saturation modeling, example from the Starfak T1 reservoir, middle Miocene Gulf of Mexico*, MS thesis, Department of Petroleum and Geosystems Engineering, University of Texas at Austin, Austin, Texas, 2005.

Hovorka, S.D., et al., Monitoring a large volume CO2 injection: Year two results from SECARB project at Denbury's Cranfield, Mississippi, USA, *Energy Procedia*, 4, 3478–3485, 2011.

Narasimhan, T.N. and P.A. Witherspoon, An integrated finite difference method for analyzing fluid flow in porous media, *Water Resources Research*, 12(1), 57-64, 1976.

Oldenburg, C.M. and C. Doughty, Injection, Flow, and Mixing of CO2 in Porous Media with Residual Gas, *Transport in Porous Media*, 90, 201–218, 2011.

Oldenburg, C.M., G.J. Moridis, N. Spycher, and K.Pruess, *EOS7C Version 1.0: TOUGH2 Module for Carbon Dioxide or Nitrogen in Natural Gas (Methane) Reservoirs*, Rep.

LBNL-56589, Lawrence Berkeley National Laboratory, Berkeley, CA, 2004.

Pruess, K., The TOUGH codes - A family of simulation tools for multiphase flow and transport processes in permeable media, *Vadose Zone Journal*, 3(3),738-746, 2004.

Pruess, K., C. Oldenburg, G. Moridis, *TOUGH2 users guide, Ver. 2.0*, Rep. LBNL-43134, Lawrence Berkeley National Laboratory, Berkeley, CA, 1999.

Pruess, K. and N. Spycher, ECO2N—A fluid property module for the TOUGH2 code for studies of CO2 storage in saline aquifers, *Energy Conversion and Management*, 48(6), 1761–1767, 2007.

Spycher, N. and K. Pruess, CO2-H2O mixtures in the geological sequestration of CO2: II Partitioning in chloride brines at 12 − 100◦C and up to 600 bars, *Geochim. Cosmochim. Ac.*, 69(13), 3309–3320, 2005.

van Genuchten MTh, A closed-form equation for predicting the hydraulic conductivity of unsaturated soils, *Soil Sci. Soc. America Journal*, 44(5), 892–898, 1980.

Vinsome, P.K.W., and J. Westerveld. A simple method for predicting cap and base rock heat losses in thermal reservoir simulators, *J. Canadian Petroleum Technology*, 87-90, July-September, 1980.